Journal of Inorganic and General Chemistry
ZAAC
Zeitschrift für anorganische und allgemeine Chemie
DOI: 10.1002/zaac.202000221
ARTICLE

Synthesis, Characterization, and Reactivity of a Series of Homo- and Hetero-dinuclear Complexes based on an Asymmetric FloH Ligand System

Beatrice Battistella,[a] Florian Heims,[a] Beatrice Cula,[a] and Kallol Ray*[a]

Dedicated to Prof. Manfred Scheer on the Occasion of his 65th Birthday

Abstract. In a previous communication we reported the site-directed generation of a heterodinuclear $Fe^{III}Cu^{II}$ complex (**1**) by using an asymmetric dinucleating ligand FloH. The iron(III) ion was introduced first on the preferential metal-binding site of the ligand that led to the formation of the thermodynamically favored five-membered chelate ring upon metal-binding. Copper(II) was introduced in the next step. The stepwise metalation strategy reported previously has now been extended to synthesize a series of heterodinuclear $Fe^{III}M^{II}$ [M = Mn (**2**), Fe (**3**), Co (**4**), and Ni (**5**)] and $Fe^{II}Cu^{I}$ (**1a**) as well as the homodinuclear $Cu^{I}Cu^{I}$ (**6**) complexes. The complexes were characterized by X-ray crystallography (except for **1a** and **6**), and by a limited number of spectroscopic methods. Complex **1** with a labile solvent binding site at Fe^{III} reacted with H_2O_2 to form a transient intermediate that showed reactivity typical of metal peroxide complexes. The metal centers in the complexes **2**–**5** are coordinatively saturated, and hence they showed no reactivity with H_2O_2. Complex **1a** reacted with O_2 via an intermolecular pathway to form a μ-oxo bridged tetrameric complex **1b**, which was structurally characterized. This is in contrast to the homodinuclear $Cu^{I}Cu^{I}$ and heme $Fe^{II}Cu^{I}$ cores, which prefer an intramolecular pathway for O_2 activation.

Introduction

Enzymatic cofactors containing two different metal centers are often used in nature to carry out a variety of important oxidative transformations.[1] These heterodinuclear active sites can exhibit alternative reactivity patterns relative to their symmetric counterparts. Hence, the synthesis and the understanding of the reactivity properties of heterodimetallic complexes are important in the context of modelling the structures and reactivities of metalloenzymes containing two different metal ions at their active sites.[1–10] However, such studies are not trivial due to the challenges associated with synthesis of heterodinuclear complexes, mainly because of the possibility of disproportionation and the formation of mixtures of homo- and heterodinuclear complexes, as well as metal-site isomers. A limited number of successful synthesis of heterodinuclear complexes involve the use of asymmetric ligands that bind metals selectively in one pocket or strongly enough to prevent disproportionation and metal mixing.[2,11–16]

For example a series of heterodimetallic $Fe^{III}M^{II}$ (M = Fe, Cu, Co, Cd, and Zn) complexes[17–20] in good yields have been synthesized by utilizing hard and anionic oxygen donors on one side to selectively bind the Fe^{III} ion, and soft and neutral nitrogen donors on the other side, to preferentially bind the divalent metal ions. A few symmetric ligands have also been successfully utilized in the synthesis of heterodinuclear complexes by treating the ligands with equimolar amounts of two different metal salts;[11] the factors that contribute to the sole formation of the heterodinuclear complexes without the contamination of the homodinuclear units are, however, not clear in these cases.[11,21] In our group we previously reported the site-directed generation of a heterodinuclear $Fe^{III}Cu^{II}$ complex **1** by using an asymmetric dinucleating ligand FloH (Scheme 1).[2]

The iron(III) ion was introduced first on the preferential metal-binding site of the ligand that leads to the formation of the thermodynamically favored five-membered chelate ring upon metal-binding.[22] Copper(II) was introduced in the next step. This stepwise metalation strategy that makes use of the different thermodynamic stabilities of the six- vs. five-membered chelate rings has now been extended in the present study for the preparation of a series of heterodinuclear $Fe^{III}M^{II}$ [M = Mn (**2**), Fe (**3**), Co (**4**), and Ni (**5**)] and $Fe^{II}Cu^{I}$ (**1a**), as well as homodinuclear $Cu^{I}Cu^{I}$ (**6**) complexes (Scheme 1). The abilities of the complexes to activate dioxygen and hydrogen peroxide have been investigated; a comparative reactivity study establishes some important differences in the oxidation mechanism depending on the nature and the oxidation state of the metal ions.

* Prof. Dr. K. Ray
E-Mail: Kallol.Ray@chemie.hu-berlin.de
[a] Institut für Chemie
Humboldt-Universität zu Berlin
Brook-Taylor Str. 2
12489, Berlin, Germany
Supporting information for this article is available on the WWW under **http://dx.doi.org/10.1002/zaac.202000221** or from the author.

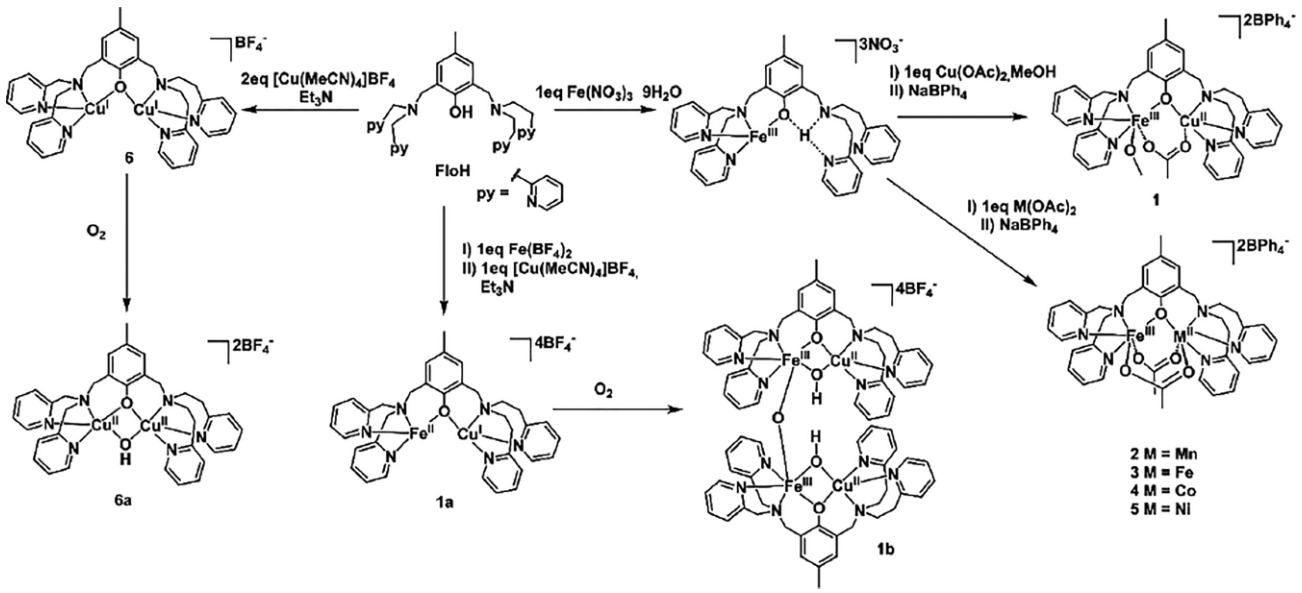

Scheme 1. Nomenclature of the synthesized complexes.

Results and Discussion

FloH Ligand: Preferential Binding of the Metal Ions to the Bis(2-pyridylmethyl)amino Site

The ligand FloH was synthesized previously and contains two metal binding sites: a preferential metal-binding site provided by the bis(2-pyridylmethyl)amino moiety and a second binding site involving the bis(2-pyridylethyl)amino group.[2] The preferential coordination of metal ions to the bis(2-pyridylmethyl)amino moiety was validated by following the reaction of a 1:1 mixture of bis(2-picolyl)(2-hydroxy-3,5-di-*tert*-butylbenzyl)amide (BPPA) and 2,4-di-*tert*-butyl-6-[[bis[2-(2-pyridyl)ethyl]amino]methyl]phenol (BAMP) with one equivalent of $Fe(NO_3)_3{\cdot}9H_2O$ or $Cu(NO_3)_2{\cdot}H_2O$ by electro-spray ionization time of flight mass spectroscopy (ESI-TOF; Figure 1). Although direct observation of the signals corresponding to the triply charged Fe^{III}(BPPA) or doubly charged Cu^{II}(BPPA) complex ions was not possible, the disappearance of the signal at *m*/*z* = 418.2834 (corresponding to BPPA containing the bis(2-pyridylmethyl)amino moiety) in presence of Fe^{III} or Cu^{II} ions can be interpreted as a result of the consumption of BPPA by complex formation. In contrast, the intensity of the signal of the free BAMP ligand at *m*/*z* = 446.3353 (containing the bis(2-pyridylethyl)amino group) remained unaffected by the addition of the metal salts under the same measurement conditions. This clearly suggests that irrespective of the nature of the metal ions, the BPPA ligand preferentially undergoes the complexation reactions.

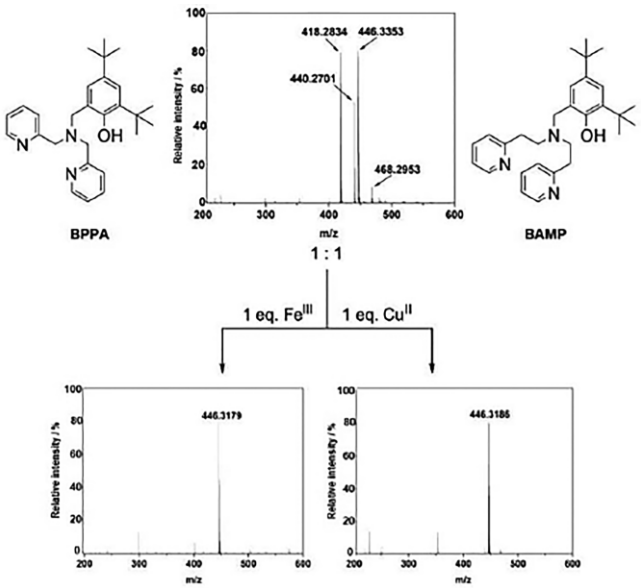

Figure 1. ESI-TOF mass spectra of a 1:1 mixture of BPPA and BAMP after the addition of one equivalent each of $Fe(NO_3)_3$ and $Cu(NO_3)_2$.

Synthesis and Characterization of 1–6

Synthesis

Reaction of FloH with $Fe(NO_3)_3$ leads to the initial binding of the Fe^{III} ion into the bis(2-pyridylmethyl)amino site with formation of a deep-blue solution containing the monoiron complex. Addition of $M(OAc)_2$ (M = Cu, Mn Fe, Co, Ni) to the resultant blue solution and subsequent anion metathesis with sodium tetraphenylborate results in the precipitation of **1**–**5**, because of the binding of M^{II} to the vacant bis(2-pyridylethyl)amino group (Scheme 1). Complex **1a** was similarly obtained by adding $Fe(BF_4)_2$ to FloH in CH_2Cl_2 under anaerobic conditions, followed by the addition of $[Cu(MeCN)_4]BF_4$ and trimethylamine. The homodinuclear Cu^ICu^I complex **6** was synthesized insitu by adding two equivalents of $[Cu(MeCN)_4]BF_4$ in presence of base to deprotonate the phenolate function, which is necessary to metalate the second coordination site (Scheme 1).

Mass Measurements

Electrospray ionization mass spectroscopic (ESI-MS) studies on **1** showed two signals at a mass-to-charge ratio (*m*/*z*) of 376.09 (calcd. *m*/*z* = 376.092 for $[C_{37}H_{41}CuFeN_6O_4]^{2+}$) and 383.10 (calcd. 383.099 for $[C_{38}H_{43}CuFeN_6O_4]^{2+}$), which based on their isotope patterns could be assigned to the heterodinuclear $Fe^{III}Cu^{II}$ core. Similarly, for **2**–**5** the expected molecular ion peaks corresponding to the heterodinuclear cores in **2**, **4**, and **5** and the mixed valent diiron core in **3** could be obtained (Table S1, Supporting Information). In particular for **2**, **4**, and **5** no signal corresponding to the diiron, dicobalt, dimanganese or diiron cores were obtained thereby suggesting the absence of any metal mixing during the complexation reactions. The extreme sensitivity of **1a** towards oxygen prevented its investigation by ESI-MS. Hence **1a** was examined by using liquid injection field desorption ionization (LIFDI) mass spectrometry (Figure S1, Supporting Information). Two intense signals corresponding to the $[(Flo)(Fe)(Cu)(F)]^+$ ($[C_{35}H_{37}CuFeFN_6O]^+$ calcd. *m*/*z*: 695, found *m*/*z*: 695) and $[(Flo)(Fe)(Cu)(F)_2]^+$ ($[C_{35}H_{37}CuFeF_2N_6O]^+$ calcd. *m*/*z*: 714, found *m*/*z*: 714) cations were observed; this corroborates the formation of the heterodinuclear $Fe^{II}Cu^{I}$ core; the F^- anion is presumably abstracted from BF_4^- under the conditions of LIFDI experiments.

Solid State Structure

The structure of **1** was reported previously,[2] and that of **2**–**5** are determined in the presented study (Figure 2). The molecular structures show the expected occupation of the five-membered chelate ring by Fe^{III} added in the first metalation step and the formation of the six-membered chelate ring by M^{II}, with both the metal ions connected by a phenolate and by one

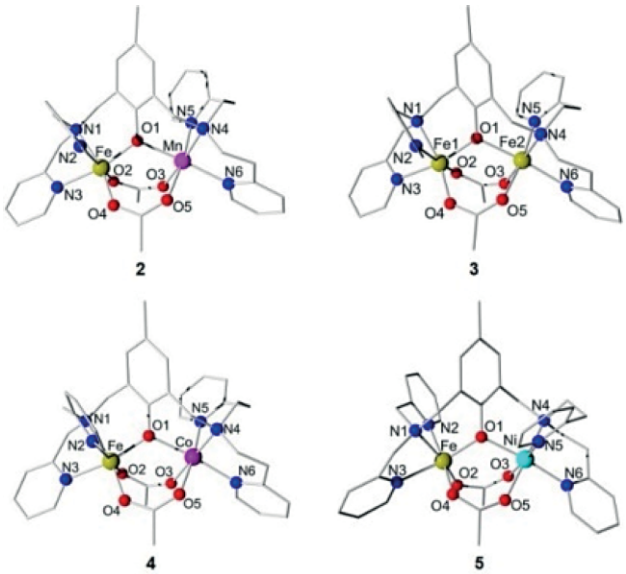

Figure 2. X-ray crystal structure of complexes **2**–**5**. Hydrogen atoms and counterions are omitted for clarity.

(for **1**) or two bridging acetate (for **2**–**5**) ligands. Thus both the metal centers in **2**–**5** are in an octahedral coordination environment involving phenolate oxygen atom, three nitrogen atoms of the bis(2-pyridylmethyl)amino or bis(2-pyridylethyl)amino moieties, and two bridging acetate groups (Figure 2). The Cu^{II} site in **1**, in contrast, is intermediate between trigonal-bipyramidal and square-pyramidal (τ = 0.52) and the Fe^{III} site attains the octahedral coordination environment by binding to an additional methoxide ligand, derived from the solvent.

The metrical parameters of the complexes are summarized in Table 1. Fe–O bond lengths in **1** vary in the range of

Table 1. Selected metal-ligand distances and angles for complexes **2**–**5**.

Bond /Å	**1** (M = Cu)	**2** (M = Mn)	**3** (M = Fe)	**4** (M = Co)	**5** (M = Ni)
Fe–O1	2.008(3)	1.939(2)	1.946(2)	1.946(1)	1.943(1)
Fe–O2	1.834(4) [a]	1.992(2)	2.009(2)	2.006(1)	1.920(2)
Fe–O4	1.999(4)	1.920(2)	1.923(2)	1.916(1)	2.007(1)
Fe–N1	2.247(4)	2.188(3)	2.201(2)	2.192(2)	2.196(2)
Fe–N2	2.133(4)	2.138(2)	2.142(2)	2.134(1)	2.145(2)
Fe–N3	2.156(4)	2.156(3)	2.171(2)	2.166(2)	2.172(2)
M–O1	1.962(3)	2.161(2)	2.152(2)	2.130(1)	2.113(1)
M–O3	1.975(4)	2.132(2)	2.105(2)	2.098(1)	2.098(2)
M–O5	–	2.222(3)	2.159(2)	2.128(2)	2.090(1)
M–N4	2.070(4)	2.310(2)	2.173(2)	2.147(1)	2.101(2)
M–N5	2.182(4)	2.265(3)	2.173(2)	2.127(2)	2.079(2)
M–N6	2.018(4)	2.222(3)	2.203(2)	2.180(1)	2.138(2)
Angle /°					
O1–Fe–O2	98.34(15) [a]	97.7(1)	94.19(7)	93.78(5)	99.69(6)
O1–Fe–O4	90.50(15)	102.3(1)	100.68(8)	100.14(5)	93.77(6)
O1–Fe–N1	86.58(14)	89.87(9)	90.30(8)	90.75(5)	90.78(6)
O1–Fe–N2	87.01(14)	88.60(9)	87.66(8)	88.11(5)	88.54(6)
O1–Fe–N3	160.15(16)	165.3(1)	165.34(8)	165.61(6)	165.42(6)
O1–M–O3	89.90(15)	89.03(8)	87.63(7)	87.64(5)	87.33(6)
O1–M–O5	–	85.14(9)	86.07(7)	86.60(5)	87.40(6)
O1–M–N4	92.32(15)	87.73(9)	91.25(7)	91.91(5)	92.49(6)
O1–M–N5	103.58(14)	88.64(9)	86.89(7)	87.42(5)	87.50(6)
O1–M–N6	145.83(16)	172.52(9)	174.63(7)	174.35(5)	174.20(6)

a) With O2 from the solvent molecule (MeOH) and O5 missing due to the coordination of only one bridging acetate in **1**.[2]

1.834(4)–2.004(4) Å, whereas the Fe–N bonds are generally longer [2.133(4)–2.249(5) Å]. For the Cu–O and Cu–N bonds similar trends are found [1.965(4)–1.976(4) Å for Cu–O and 2.014(5)–2.183(4) Å for Cu–N].[2] The trend of shorter Fe–O and longer Fe–N distances is also observed in **2**–**5**. The Mn–O/N bonds in **2** vary between 2.132(2) and 2.310(2) Å, which are comparable to the reported bond lengths in the heterobimetallic $Fe^{III}Mn^{II}$ complex [FeMn(L-Bn)(μ-OAc)$_2$](ClO$_4$) (^{l}-Bn = {[2-bis[(2-pyridylmethyl)aminomethyl]]-6-[benzyl-2-(pyridylmethyl) aminomethyl]-4-methylphenolate) from the groups of *Blondin*, *Latour* and co-workers.[23]

Similarly, for **4**, the observed metrical parameters match well to that previously reported in the Phosphatidate phosphatase (PAP) model complex [FeCo(BPBPMP)(μ-OAc)$_2$]ClO$_4$ by *Neves* and co-workers.[24] The observed bond lengths in **5** [Fe–O 1.920(2)–2.007(1) Å, Fe–N 2.145(2)–2.196(2) Å and Ni–O 2.090(1)–2.113(1) Å, Ni–N 2.079(2)–2.138(2) Å] also fit to the metrical parameters of the known $Fe^{III}Ni^{II}$ complexes in the literature.[25,26] In the case of **3** the different oxidation states of the two iron cores can be crystallographically discriminated, exploiting the different bond lengths between the O-donor functions and the iron ions. A higher positive charge on Fe leads to a shortening of the bond, in particular to a *hard* moiety such as O-donor functions. As expected, Fe–O bond lengths of 1.923(2)–2.009(2) Å are found on the 5-member chelate ring, which on average are 0.1–0.2 Å shorter than the corresponding Fe–O bond lengths [2.105(2)–2.159(2) Å] found in the six-membered chelate ring, where the Fe^{II} binds.

Energy Dispersive X-ray (EDX) Spectroscopic Measurements

To confirm the selective formation of the heterodinuclear complexes, EDX measurements were carried out on single-crystals of **1**, **2**, **4**, and **5**. In each case it could be shown that both elements exist side by side in a single crystal, with the iron signal observed at 6.4 keV in all cases and a second signal depending on the nature of the second metal ion [Cu = 8.0 keV (**1**); Mn = 5.9 keV (**2**), Co = 6.9 keV (**4**) and Ni = 7.5 keV (**5**)] (Figure S2, Supporting Information).

IR Measurements

The IR spectrum of **1** shows two intense signals for the symmetric (ν_{sym}) and antisymmetric (ν_{anti}) carboxylate stretching frequencies of the bridging acetate at 1559 cm^{-1} and 1428 cm^{-1}, respectively.[2] The difference between ν_{anti} and ν_{sym} ($\Delta\nu = \nu_{anti} - \nu_{sym}$) is 131 cm^{-1}, which are characteristic for bridging carboxylate ligands. Comparison of these symmetric (1550 cm^{-1}, ν_4) and antisymmetric stretches (1425 cm^{-1}, ν_2) of the bridging carboxylates for **2** (FeMn), **3** (FeFe), **4** (FeCo), and **5** (FeNi) reveal only minor differences despite their bridging between different metals and the involvement of different number of carboxylates (Table S2, Supporting Information).[15,23–26] This implies that the structures of the Fe^{III} M^{II} (M = Cu, Mn, Fe, Co, Ni) cores remain unaltered in **1**–**5**, which is also supported by the overlay of their X-ray structures.

Magnetic Properties

The overall effective magnetic moment (μ_{eff}) of **1** was determined previously by NMR spectroscopy using the Evans method at 298 K.[2,27] The obtained experimental value of 5.24 μ_B (calcd. spin-only effective magnetic moment $\mu_{eff} = g\sqrt{S_{Fe}(S_{Fe}+1) + S_{Cu}(S_{Cu}+1)} = 6.17\ \mu_B$, where g = gyromagnetic ratio = 2.00023 μ_B, S_{Fe} and S_{Cu} = spins at Fe and Cu, respectively[28]) and Mössbauer studies at 3.0 K and 4.0 T were shown to be consistent with the presence of high spin Fe^{III} and Cu^{II} centers that are weakly antiferromagnetically coupled with each other to give a S = 2 ground state (Figure S3, Supporting Information). The DFT calculated[2] magnetic exchange coupling of –58.6 cm^{-1}, is in reasonable agreement with that previously reported for related systems[29] The μ_{eff} values of **2** and **4** were similarly determined to be 8.38 and 7.08 μ_B at 298 K, which are close to the theoretical spin-only values expected for high spin $Fe^{III}Mn^{II}$ and $Fe^{III}Co^{II}$ cores, respectively (Table S3, Supporting Information). As previously reported, the Mössbauer spectrum of **1** shows an asymmetric doublet with an isomer shift of δ = 0.48 mm·s^{-1} and ΔE_Q = 1.16 mm·s^{-1}, which confirms the high-spin Fe^{III} assignment (Figure 3A).[2] The Mössbauer spectrum of **1a** in contrast features a symmetric doublet with δ = 1.17 mm·s^{-1} and ΔE_Q = 3.04 mm·s^{-1}, which are characteristic features of a high spin Fe^{II} center (Figure 3B).[30,31]

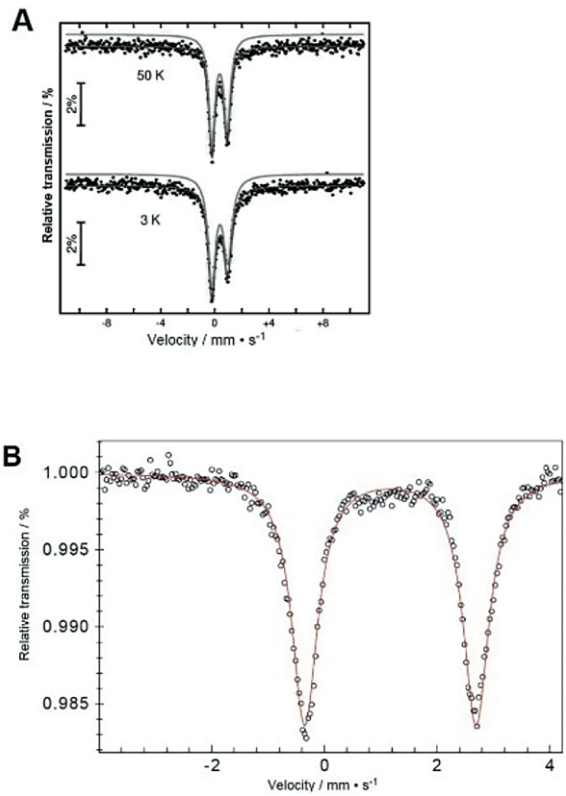

Figure 3. Solid state ^{57}Fe Mössbauer spectrum of complex **1** (A) and complex **1a** (B).

Cyclic Voltammetry

2, **4**, and **5** show a reversible reduction wave between –0.35 and –0.60 V against Fc/Fc$^+$, which has been assigned to the

Fe^{III}/Fe^{II} reduction couple (Figure 4 and Figure S4, Supporting Information). In contrast, no reversible reduction process was observed in the CV of **1**. No CV could be measured for **3** as it underwent fast decay in solution. Notably, Fe^{III}/Fe^{II} redox couple shifts towards more negative potentials on going from **2** to **4** and to **5**, which may reflect a more favorable reduction of the $Fe^{III}M^{II}$ core with increasing electronegativity of the divalent ion partner from Mn^{II} to Co^{II} and to Ni^{II}.[32] The reason why complex **1** does not follow this trend can possible be explained by the differences in the Fe and Cu coordination spheres (bound solvent molecule at Fe and five coordination at Cu), which possibly prevent or complicate the reduction of the $Fe^{III}Cu^{II}$ core.

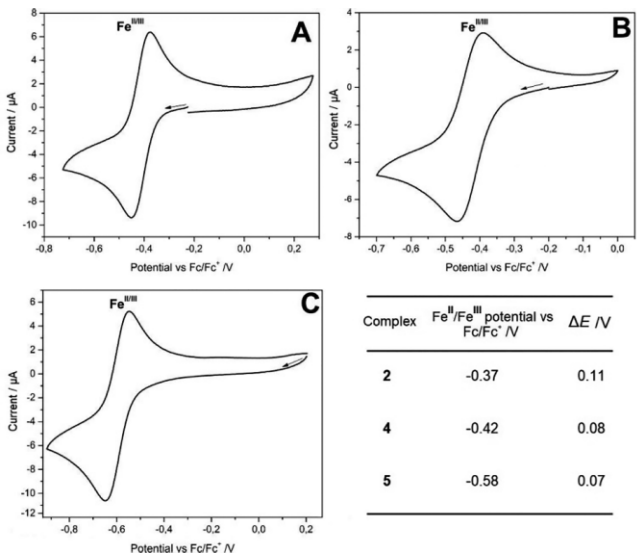

Complex	Fe^{II}/Fe^{III} potential vs Fc/Fc$^+$ /V	ΔE /V
2	-0.37	0.11
4	-0.42	0.08
5	-0.58	0.07

Figure 4. Cyclic voltammograms of complexes **2** (A), **4** (B), **5** (C) and tabular comparison of their Fe^{II}/Fe^{III} redox potentials. ΔE represents the difference in the peak positions of the oxidation (Ep_a) and reduction (Ep_c) waves. The CVs. in the extended range of 0.0–1.5 V for **1**, **2**, **4**, and **5** are shown in Figure S4 (Supporting Information).

Reactivity Studies

Reaction with H_2O_2

The successful synthesis of complexes **1**–**5** in pure form, attested by different analytic techniques, gave us the chance to investigate their reactivity towards hydrogen peroxide. Unfortunately, only complex **1** containing a labile solvent molecule at the iron(III) site showed reactivity with H_2O_2. When **1** was reacted with a mixture of ten equivalents of H_2O_2 and five equivalents of triethylamine at –45 °C, the formation of a metastable species with an absorption maximum at λ_{max} = 398 nm (ε = 2400 L·mol^{-1}·cm^{-1}) was observed. Investigation of the temperature-sensitive species (t½ = 19 min at –20 °C) by low-temperature ESI-MS, low-temperature IR spectroscopy and resonance Raman spectroscopy (rR) could not detect the formation of any peroxo intermediate. However, it showed the typical nucleophilic reactivity of a peroxo complex. For example, the reaction of this intermediate species with cyclohexane carboxaldehyde (CCA) in EtCN at –45 °C, was evident from the decay of the characteristic 398 nm band, which followed a pseudo first order behavior (Figure 5). A second-order rate constant (k_2) of 2.21×10^{-1} M^{-1}·s^{-1} (Figure 5) was determined for the reaction. Analysis of the reaction mixture by NMR studies showed the formation of cyclohexene in 10 % yield.

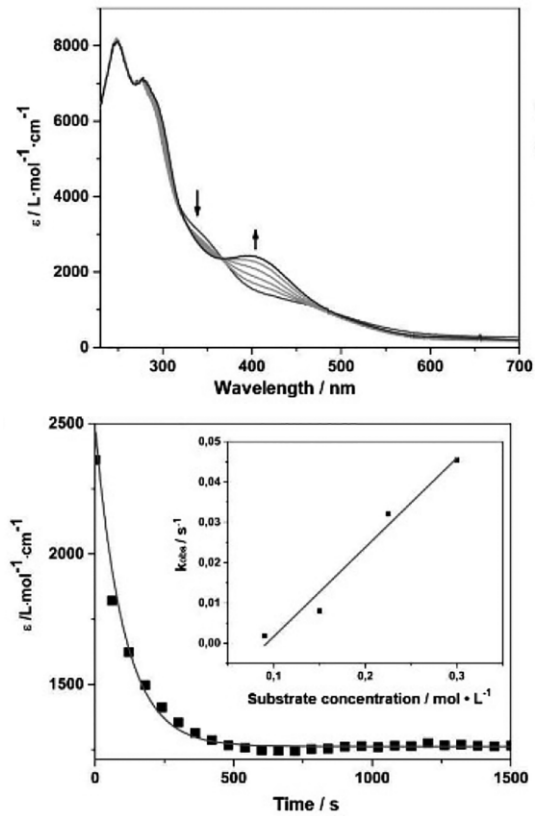

Figure 5. Changes in the UV/Vis spectrum of **1** (0.33 mM, EtCN, –45 °C) after the addition of 10 equiv. H_2O_2 / 5 equiv. NEt_3 (top); time-trace showing the first order decay of the band at 398 nm corresponding to the peroxo intermediate in the presence of cyclohexane carboxaldehyde (0.14 mol·L^{-1}) (bottom) and variation of the first-order rate constant (k_{obs}) at different CCA concentrations (inset).

The nucleophilic character of the intermediate formed upon H_2O_2 reaction is typical of metal peroxide compounds.[33–35] However, since its nature could not be determined spectroscopically, two possible metal peroxo-structures can be hypothesized (Scheme 2). The Fe^{III} containing a labile solvent molecule is the most probable binding site for the peroxo moiety to generate a terminal $(O_2)Fe^{III}Cu^{II}$ or bridged $Cu^{II}Fe^{III}(\mu\text{-}O_2)Fe^{III}Cu^{II}$ cores. Notably, the saturated coordination environment of Cu^{II} makes it a less likely binding site for O_2^{2-}.

Reaction with O_2

The presence of two bridging acetate ligands in **2**–**5** make the metal centers coordinative saturated, which attributes to their lack of reactivity towards H_2O_2. Complex **1** showed intermediate reactivity because of the presence of one labile solvent binding site at Fe^{III}. Unsaturation of the metal sites is therefore a prerequisite to achieve high reactivity of the complexes.

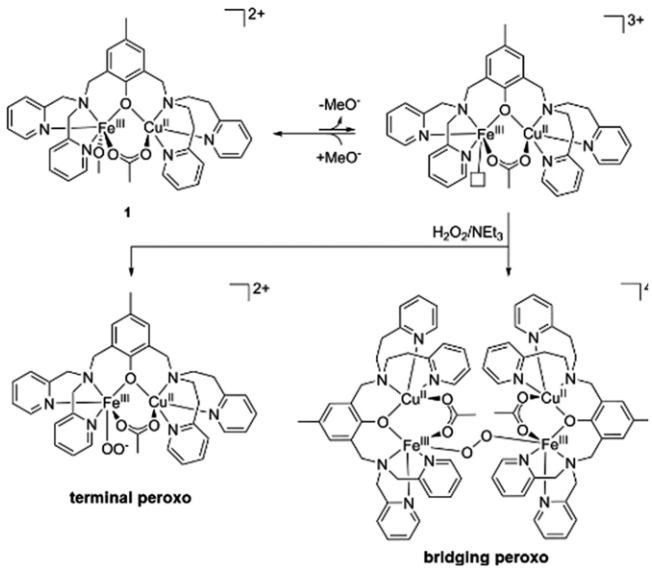

Scheme 2. Proposed structures of the intermediate peroxo species that may result from the reaction of **1** with 10 eq hydrogen peroxide and 5 equiv. triethylamine.

However, all our attempts to synthesize the $Fe^{III}M^{II}$ complexes in presence of non-coordinating counteranions like PF_6^- or BF_4^- proved unsuccessful. Nevertheless, the synthesis of complex **1a** containing a reduced $Fe^{II}Cu^{I}$ center in the absence of any bridging carboxylate ligand was possible, which gave us the option to investigate its reactivity in presence of dioxygen. An acetonitrile solution of **1a**, when reacted towards O_2, revealed an instant color change from orange to deep red. Single crystals suitable for X-rays structure analysis of this new compound, complex **1b**, were obtained, and the structure is shown in Figure 6A.

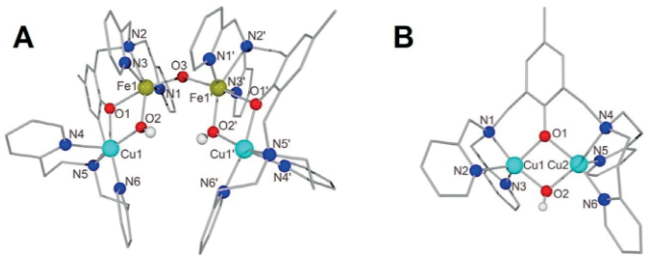

Figure 6. Molecular structures of **1b** (A) and **6a** (B) in the solid state. Carbon-bound hydrogen atoms and counterions are not shown for reasons of clarity.

Complex **1b** presents a tetrameric structure with the two Fe^{III} ions being situated in a distorted octahedral coordination environment and two Cu^{II} ions in a distorted square-pyramidal (τ = 0.21) geometry. Consistent with the previous metalation experiments, Fe forms a five-membered chelate ring with the N-donor functions of the ligand, while Cu forms a six-membered chelate ring. The Fe and Cu centers are linked by bridging phenolate and hydroxide units, whereas a μ-oxo bridge connects the two Fe^{III} centers (Figure 6A). The Cu–O1 [1.956(3) Å], Cu–N [Cu1–N4 2.259(3) Å, Cu1–N5 2.079(3) Å, Cu1–N6 1.992(3) Å] and Fe–N [Fe1–N1 2.165(3) Å, Fe1–N2 2.232(3) Å, Fe1–N3 2.169(3) Å] bond lengths in **1b** are similar to that observed in **1** (Table 1).[2] The Fe–O bonds are, however, slightly elongated at 1.960(3) and 2.133(2) Å (Table 1). The Fe–O–Fe core features slightly shorter Fe–O distance (1.792 Å) than the Fe–O1 and Fe–O2 bonds. The observed bond angle and the bond lengths of the Fe–O–Fe structural motif in **1b** are consistent with dinuclear oxido-bridged Fe^{III} complexes known in the literature.[36–39] The oxygen atom O3 is located on a crystallographic inversion center, therefore the bond lengths and angles are identical in the two heterodinuclear subunits. The Mössbauer spectrum of **1b** shows a doublet with δ value of 0.49 mm·s^{-1} and ΔE_Q of 1.44 mm·s^{-1} very similar to **1** (Figure S5, Supporting Information; some residual **1a** is also observed in the Moessbauer spectrum).

The ESI-MS spectrum of **1b** shows two signals at m/z = 1663.345 and 788.171, corresponding to the $[C_{70}H_{76}B_3Cu_2F_{12}Fe_2N_{12}O_5]^+$ and $[C_{70}H_{76}B_2Cu_2F_8Fe_2N_{12}O_5]^{2+}$ ions, respectively. These signals get shifted by 2 and 1 units respectively (at m/z = 1665.3471 and 789.1725) when $^{18}O_2$ was used for the synthesis of **1b**, thereby showing only one oxygen atom from a dioxygen molecule is incorporated in **1b** (Table S5, Supporting Information). However, we tentatively assign both the μ-oxo and μ-hydroxo bridges to be derived from dioxygen; the hydroxo bridge then exchanges with residual water in the reaction mixture under the conditions of ESI-MS. The IR spectra of **1b** (Figure S6, Supporting Information) reveal an intense vibration at 1087 cm^{-1}, which upon ^{18}O labeling gives rise to a doublet at 1051 cm^{-1} and 1021 cm^{-1}. An assignment of this vibration is beyond the scope of the present manuscript; the energy of the vibration falls in the region of ν(OH) out of plane deformation,[40,41] although, the observed large isotopic shift upon ^{18}O labeling is inconsistent with such an assignment.

In order to compare the effect of metal substitution in the oxygen activation process, the O_2 activation reaction of the corresponding $Cu^{I}Cu^{I}$ complex **6** was also studied. The resultant product **6a**, could be isolated and structurally characterized by X-ray diffraction method (Figure 6B) as a hydroxo-bridged dicopper(II) complex. The metrical parameters in **6a** compare well to that of the μ-hydroxido-dicopper(II) complex reported by *Karlin* and co-workers, which was also obtained by oxidation of the corresponding dicopper(I) complex with O_2.[42] The formation of the Cu^{II}–μ-O(H)–Cu^{II} (**6a**) complex shows the preference of a dicopper center for a cooperative O_2-reactivity via an intramolecular mechanism, in contrast to the Fe^{I}-$^{I}Cu^{I}$ complex **1a**, that activates dioxygen via an intermolecular pathway.

Conclusions

In addition to mono- and homodinuclear active centers, there are also enzymes that utilize heterodinuclear active centers to carry out a variety of oxidative reactions. Each individual metal ion plays a defined role in these enzymes during the catalytic cycle. The synthesis of model complexes for such asymmetric systems is much more demanding than that of the homometallic analogues, since side reactions like dispropor-

tionation, isomer formation and selectivity problems must be prevented during the metalation process. Two major strategies have been followed in the past to achieve this goal. The first strategy involves the independent synthesis of mononuclear precursor compounds with different metal ions, which are then reacted with each other to achieve the heterometallic cores.[43–49] The second strategy involves the synthesis of ligand precursors with two different coordination pockets, which can be addressed selectively in the metalation process. Following the latter strategy, the ligand system FloH was developed, which contains two metal binding sites involving 2-bispyridyl methylamine and 2-bispyridyl ethylamine donor groups. Since five-membered chelate rings are thermodynamically more stable, preferential metalation occurs at the 2-bispyridyl methylamine site, leaving the second coordination pocket accessible for the second metal ion. Using this synthetic strategy, a library of heterodinuclear $Fe^{III}M^{II}$ (M = Mn, Fe, Co, Ni, Cu) and $Fe^{II}Cu^{I}$ as well as homodinuclear $Cu^{I}Cu^{I}$ complexes could be synthesized and characterized (Scheme 1). The $Fe^{III}M^{II}$ complexes could be stabilized only in presence of bridging acetate ligands, which saturated the coordination sphere of the metal ions to an extent that the complexes showed no or limited reactivity towards organic peroxides. Attempts to selectively protonate the complexes to remove the acetate ligand from the metal centers, led to protonation of the phenolate function of the ligand and the subsequent release of the M^{II} ion, as has been demonstrated previously for **1**.[2]

The reduced $Fe^{II}Cu^{I}$ complex **1a** was also synthesized in an effort to investigate the dioxygen activation ability of the heterodinuclear core. A detailed characterization of **1a** was hampered by its fast reaction with oxygen to form the tetranuclear complex **1b** that contained two $Fe^{III}Cu^{II}$ cores connected by a Fe^{III}–O–Fe^{III} bridge. Thus in contrast to heme-based, heterobimetallic $Fe^{II}Cu^{I}$ model complexes (e.g. cytochrome c oxidase model systems)[50–53] that tend to bind and activate oxygen intramolecularly, non-heme-based $Fe^{II}Cu^{I}$ systems seem to activate oxygen preferentially by an intermolecular pathway (Scheme 3). The large thermodynamic stability of the

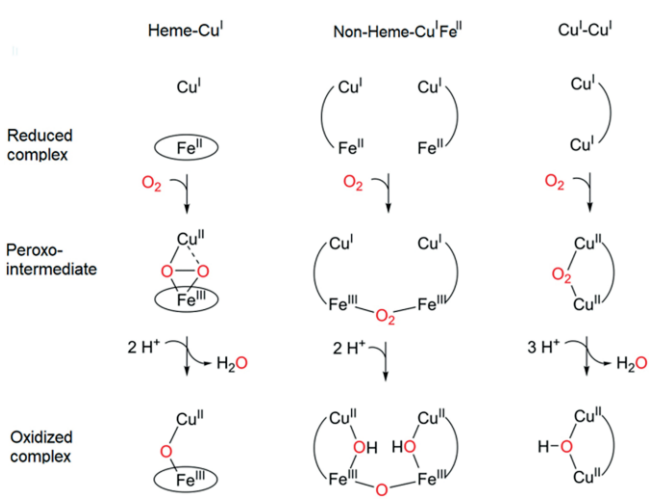

Scheme 3. Different dioxygen mechanisms of heme $Fe^{II}Cu^{I}$, non-heme $Fe^{II}Cu^{I}$, and $Cu^{I}Cu^{I}$ cores.

Fe^{III}–O–Fe^{III} moiety presumably provides the driving force for the intermolecular pathway. Notably, the corresponding dicopper(I) complex **6**, which was formed by reaction of FloH with two equivalents of a Cu^{I} salt, activtes O_2 by the intramolecular reaction pathway to form the μ-hydroxide-bridged dicopper(II) complex **6a**, which was isolated and structurally characterized (Figure 6B). Therefore, we conclude that non-heme-based iron-copper systems represent a borderline case of oxygen activation at bimetallic centers, where a steric prevention of the intermolecularly bridged Fe^{III}–O–Fe^{III} complex is necessary to achieve O_2 activation at the heterodinuclear $Fe^{II}Cu^{I}$ center.

Experimental Section

General: All reagents were purchased from Sigma Aldrich, ABCR, Acros and TCI Europe and used as received, unless otherwise mentioned. The UV/Vis absorption spectra were recorded with an 8453 UV/Vis SPECTROSCOPY SYSTEM from AGILENT. The measurements were carried out in 10 mm and 5 mm precision cuvettes made of SUPRASIL® quartz glass, the closures of which were equipped with a septum. The measurements at low temperatures were carried out by cooling the cuvette holder using a USP-203-A cryostat from UNISOKU SCIENTIFIC INSTRUMENTS. The analysis of the spectra was carried out with the software UV/Vis CHEMSTATION from AGILENT. For a typical UV/Vis experiment, two milliliters of a solution of the complex with a known concentration was prepared in a glove box and transferred to a cuvette that is closed with a septum. The cuvette was then placed in a thermostat and the solution is continuously stirred until it reaches a thermal equilibrium. The reactant solutions were prepared in a minimum amount of solvent and then injected into the cuvette through a septum using a syringe. The changes in the UV/Vis spectrum were then recorded. The specified molar extinction coefficients (ε) of the specific absorption maxima (λ_{max}) are mean values of several individual measurements. The lifetime (t½) of an intermediate or complex was followed by the decrease in the specific absorption characteristics of the intermediate species over time at a certain temperature. The kinetics of the decay of the peroxo intermediate was determined analogously by following the decrease in the characteristic absorption band at 398 nm in presence of external substrates under pseudo-first order conditions. The pseudo-first-order rate constants (k_{obs}) were found to be linearly proportional to the substrate concentrations. The second-order rate constant (k_2) is determined by the slope of the linear plot. Electrospray ionization mass spectrometry experiments were carried out with a Finnigan LTQ fourier transform ion cyclotron resonance mass spectrometer (Therma Electron Co. Bremen). The "liquid injection field desorption ionization" (LIFDI) mass spectra were recorded on a MICROMASS Q-TOF-2 instrument with a LIFDI ionization unit from LINDEN CMS. The EDX spectrum was measured with a Quantax system (Röntec) in ultra-high vacuum (UHV; 10^{-7} mbar) with an energy-dispersive Si-Li detector attached to a scanning electron microscope JSM 6060 (Joel). ICP analyses were obtained with a VISTA-MPX CCD Simultaneous ICP-OES spectrometer (Varian); the solutions were prepared by extraction of **1–5** by heating a suspension of about 8 mg of the complexes, 2.5 mL of conc. HNO_3 and 0.5 mL of H_2O_2 (30 %) in a microwave oven (MLS easywave) at 200 °C for 45 min, followed by dilution with deionized water. All infrared spectroscopic measurements were carried out in an FTIR-8400S infrared spectrometer with dry air purging from SHIMADZU in a range of 4000–550 cm^{-1} with a resolution of 2 cm^{-1}. The frequency specifications [in cm^{-1}] apply to the position of the maxima of the infrared absorption bands. The samples were measured in the form of

a potassium bromide pellet which had previously been prepared in an agate mortar. Cyclic voltammograms were recorded at room temperature under Ar atmosphere in acetonitrile solutions in presence of 0.1 mol·L^{-1} NBu_4PF_6 as a supporting electrolyte. The potential was set by a potentiostat/galvanostat Reference600 from Gamry Instruments. A typical CV experiment consisted of a cell equipped with a platinum working electrode, a platinum counter electrode and a platinum or silver wire as a pseudo reference electrode. At the end of each series of measurements, all recorded spectra were referenced against the ferrocene/ferrocenium redox couple. The scan rates were between 10–100 mV·s^{-1}. The Mössbauer spectra were acquired by using a conventional spectrometer in the constant-acceleration mode equipped with a ^{57}Co source (3.7 GBq) in a rhodium matrix. Isomer shifts are given relative to α-Fe at room temperature. The sample was inserted inside an Oxford Instruments Mössbauer-Spectromag 4000 Cryostat, which has a split-pair superconducting magnet system with the field of the sample oriented perpendicular to the γ-ray direction, while the sample temperature can be varied between 3.0 and 300 K. 3 K temperature could be achieved by pumping the sample space. Fits of the Mössbauer spectra were obtained with the NORMOS program.[54] ^{1}H NMR were measured with a Bruker DPX-300 (300 MHz) NMR spectrometer. The spin state of **2**, **5**, **6** were determined by using the modified ^{1}H NMR method of Evans at room temperature.[27] All elemental analyses were performed by the analytical service of the Institut für Chemie of the Humboldt-Universität zu Berlin. The percentages of carbon, hydrogen, nitrogen, and sulfur were determined using a HEKAtech EURO EA 3000 analyzer. The reported values are the result of an average of two independent measurements, except for Fluorine analysis, where only one measurement was performed.

X-ray Crystallography: The crystal-structure determination was performed at 100 K with a Stoe IPDS 2T diffractometer by using Mo-K_α (K_1 and K_2 not resolved, λ = 0.71073 Å) with a variable scan width. The radiation source was a sealed X-ray tube with graphite monochromator. The reflections of the X-rays diffracted from the single crystals were registered with the single crystal diffractometers IPDS and IPDS 2T (simultaneous registration of the refractive reflections with an imaging plate, a plate sensitive to soft X-rays) from the company STOE & CIE. After the measurement and data reduction had been completed, the background, Lorentz and polarization effects were corrected. The absorption correction (empirical, numerical or spherical) was carried out with the SHELXL-97 program.[55, 56] The structures were solved by direct methods (SHELXS-2014) and refined against F^2 using the full-matrix least-squares method (SHELXL-2018). All non-hydrogen atoms were refined anisotropically. The positions of the hydrogen atoms were calculated in an ideal geometry (Reiter model). The graphic representation was done with the program DIAMOND.

Crystallographic data (excluding structure factors) for the structures in this paper have been deposited with the Cambridge Crystallographic Data Centre, CCDC, 12 Union Road, Cambridge CB21EZ, UK. Copies of the data can be obtained free of charge on quoting the depository numbers CCDC-2004701, CCDC-2004702, CCDC-2004703, CCDC-2004704, CCDC-2004705, and CCDC-2004706. (Fax: +44-1223-336-033; E-Mail: deposit@ccdc.cam.ac.uk, http://www.ccdc.cam.ac.uk)

Syntheses of Ligand FloH and Complex 1: Ligand FloH and complex **1** have been synthesized according to literature.[2]

General Procedure for the Synthesis of [(Flo)Fe^{III}M^{II}(OAc)$_2$]$^{2+}$ (2–5): To a solution of FloH in MeOH was added $Fe(NO_3)_3$·$9H_2O$ (1 equiv.) in MeOH. The reaction mixture was stirred at room temperature for 18 h. After that time, $M(OAc)_2$ (1 equiv.) in MeOH was added, and the mixture was stirred again at room temperature for 10 h. $NaBPh_4$ (3 equiv.) in MeOH was then added, and a precipitate was formed immediately. After stirring for 10 h, the precipitate was filtered, washed with a small amount of MeOH and dried in vacuo to obtain complexes **2–5** as solid in good yield (72–89 %). Crystals suitable for X-ray diffraction analysis were obtained by recrystallization from a CH_2Cl_2/MeOH solution.

Characterization of 2: $C_{87}H_{83}B_2FeMnN_6O_5$ (M = 1425.06 g·mol^{-1}): calcd. C 73.33, H 5.87, N 5.90 %; found: C 73.75, H 5.91, N.5.99 %. **ESI-MS** (*m*/*z*): $[C_{38}H_{43}FeMnN_6O_{42}]^+$ calcd.: 393.101, found: 393.101. **IR** (KBr): $\tilde{\nu}$ = 3440 (br.), 3055 (m), 3036 (m), 2998 (m), 2983 (m), 2920 (w), 1606 (s), 1580 (m), 1570 (m), 1478 (s), 1441 (m), 1426 (m), 1413 (m), 1408 (m), 1385 (m), 1333 (m), 1160 (w), 1022 (w), 732 (s), 704 (s), 612 (m) cm^{-1}. μ_{eff} = 7.96 μ_B (Evans-Method, CD_2Cl_2, 298 K, calcd.: μ_{eff} = 8.38 μ_B).

Characterization of 3: $C_{87}H_{83}B_2Fe_2N_6O_5$ (M = 1425.97 g·mol^{-1}): calcd. C 73.28, H 5.87, N 5.89 %; found: C 71.63, H 5.87, N 5.85 %. **ESI-MS** (*m*/*z*): $[C_{39}H_{43}Fe_2N_6O_5]^{2+}$ calcd.: 393.599, found: 393.599; $[C_{39}H_{43}Fe_2N_6O_5]^+$ calcd.: 787.199, found: 787.197. **IR** (KBr): $\tilde{\nu}$ = 3055 (s), 3036 (s), 2998 (s), 2983 (s), 2922 (w), 2858 (w), 2821 (w), 1944 (w), 1880 (w), 1817 (w), 1606 (s), 1580 (s), 1569 (m), 1478 (s), 1442 (s), 1426 (s), 1331 (m), 1262 (m), 1161 (w), 1052 (w), 1022 (m), 768 (m), 730 (s), 704 (s), 655 (w), 648 (w), 613 (m) cm^{-1}.

Characterization of 4: $C_{87}H_{83}B_2CoFeN_6O_5$ (M = 1429.06 g·mol^{-1}): calcd. C 73.12, H 5.85, N 5.88 %; found: C 73.11, H 5.87, N 6.12 %. **ESI-MS** (*m*/*z*): $[C_{39}H_{43}CoFeN_6O_5]^{2+}$ calcd.: 395.099, found: 395.098. **IR** (KBr): $\tilde{\nu}$ = 3433 (br.), 3054 (s), 3036 (s), 2998 (m), 2983 (m), 2918 (w), 2859 (w), 1606 (s), 1580 (s), 1570 (s), 1478 (s), 1443 (s), 1426 (s), 1403 (s), 1386 (s), 1342 (m), 1304 (m), 1289 (m), 1263 (m), 1160 (m), 1022 (m), 765 (s), 732 (s), 702 (s), 612 (s) cm^{-1}. μ_{eff} = 6.17 μ_B (Evans-Method, CD_2Cl_2, 298 K, μ_{eff} = 7.08).

Characterization of 5: $C_{87}H_{83}B_2FeN_6NiO_5$ (M = 1428.82 g·mol^{-1}): calcd. C 73.13, H 5.86, N 5.88 %; found: C 73.48, H 5.63, N 5.92 %. **ESI-MS** (*m*/*z*): $[C_{38}H_{43}FeN_6NiO_4]^{2+}$ calcd.: 394.600, found: 394.599. **IR** (KBr): $\tilde{\nu}$ = 3055 (s), 3036 (s), 2999 (s), 2983 (s), 2920 (m), 2862 (m), 2360 (w), 2333 (w), 1945 (w), 1882 (w), 1819 (w), 1608 (s), 1580 (s), 1570 (s), 1478 (s), 1444 (s), 1403 (s), 1385 (s), 1344 (m), 1305 (m), 1289 (m), 1263 (m), 1246 (m), 1161 (m), 1023 (s), 938 (w), 865 (w), 842 (w), 766 (m), 732 (s), 704 (s), 659 (m), 649 (m), 613 (s), 583 (w) cm^{-1}.

Synthesis of [(Flo)Fe^{III}Cu^{II}(μ-OH)]$_2$(μ-O)}(BF$_4$)$_2$ (1b): $Fe(BF_4)_2$·$6H_2O$ (27 mg, 81 µmol) was added to a solution of FloH (50 mg, 90 µmol) in anhydrous MeCN (5 mL), whereupon the solution turned orange. After stirring for 3 h at room temperature, a solution of $[Cu(MeCN)_4]BF_4$ (23 mg, 81 µmol) and triethylamine (27.5 µL, 198 µmol) in MeCN (2 mL) was added and stirring was continued for 5 h. The solvent was removed under reduced pressure, the residue was taken up in CH_2Cl_2, and the reduced form of the FeCu complex **1a** was precipitated with an excess of Et_2O as a green solid. This was then taken up again in MeCN and exposed to an O_2 atmosphere, whereupon the solution immediately turned red. The reaction mixture was evaporated to dryness, the residue was extracted in CH_2Cl_2 and precipitated with Et_2O. The resulting precipitate was filtered and dried. A red solid was obtained in 68 % yield (98 mg, 56 µmol). Single crystals suitable for X-ray crystal structure analysis could be obtained from a mixture of MeCN/Et_2O.

Characterization of 1b: $C_{70}H_{76}B_4Cu_2F_{16}Fe_2N_{12}O_5$·$2CH_2Cl_2$ (M = 1921.31 g·mol^{-1}): calcd. C 45.01, H 4.20, N 8.75 %; found: C 44.87, H 4.30, N 9.05 %. **ESI-MS** (*m*/*z*): $[C_{70}H_{76}B_3Cu_2F_{12}Fe_2N_{12}O_5]^+$

calcd.: 1663.344, found: 1663.345; $[C_{70}H_{76}B_2Cu_2F_8Fe_2N_{12}O_5]^{2+}$ calcd.: 788.171, found: 788.171; $[C_{70}H_{76}BCu_2F_4Fe_2N_{12}O_5]^{3+}$ calcd.: 496.446, found: 496.446; $[C_{70}H_{76}Cu_2Fe_2N_{12}O_5]^{4+}$ calcd.: 350,584, found: 350.584. **ESI-MS** ($^{18}O_2$ oxidation) (*m/z*) $[C_{70}H_{76}B_3Cu_2F_{12}Fe_2N_{12}O_4{}^{18}O]^+$ calcd.: 1665.3483, found: 1665.3471, $[C_{70}H_{76}B_2Cu_2F_8Fe_2N_{12}O_4{}^{18}O]^{2+}$ calcd.: 789.1727, found: 789.1725. **IR** (KBr): $\tilde{\nu}$ = 3548 (br), 3150 (br), 2986 (w), 2923 (w), 1608 (s), 1571 (w), 1481 (s), 1445 (s), 1312 (w), 1284 (m), 1162 (m), 1087 (s, br), 812 (m), 770 (m), 519 (w) cm^{-1}.

Synthesis of $[(Flo)Cu^{II}\ Cu^{II}(\mu\text{-}OH)](BF_4)_2$ (6): To a solution of FloH (34 mg, 61 µmol) in acetonitrile (5 mL) was added $[Cu(MeCN)_4]BF_4$ (40 mg, 122 µmol) in acetonitrile (2 mL), together with anhydrous triethylamine (10 µL, 74 µmol). The orange solution was stirred in an argon atmosphere at room temperature for 18 h, then the solvent was saturated with O_2 and a rapid color change from orange to green was observed. The reaction mixture was then concentrated, the residue extracted in CH_2Cl_2 and precipitated with Et_2O. The resulting green solid was filtered off and dried, obtaining the product in 34 % yield (18 mg, 21 µmol). Single crystals suitable for X-ray crystal structure analysis could be obtained from a mixture of CH_2Cl_2/Et_2O.

Characterization of 6a: $C_{35}H_{38}B_2Cu_2F_8N_6O_2{\cdot}CH_2Cl_2$ (M = 952.65 g·mol^{-1}): calcd. C 45.02, H 4.20, N 8.75; found: C 45.32, H 4.25, N 9.03. **ESI-MS** (*m/z*): $[C_{35}H_{38}Cu_2N_6O_2]^{2+}$ calcd.: 350.082, found: 350.081; $[C_{35}H_{37}ClCu_2N_6O]^{2+}$ calcd.: 359.065, found: 359.064 (after chloride extraction from the solvent). **IR** (KBr): $\tilde{\nu}$ = 3415 (br), 3067 (m), 3027 (m), 2919 (m), 2861 (m), 2096 (w), 1608 (s), 1570 (m), 1483 (s), 1443 (s), 1382 (w), 1306 (m), 1281 (m), 1257 (m), 1155 (s), 1056 (s, br), 958 (m), 865 (w), 818 (w), 770 (s), 652 (w), 638 (w), 533 (m), 521 (m) cm^{-1}.

Supporting Information (see footnote on the first page of this article): The Supporting Information for this article contains the LIFDI spectrum of **1a**, EDX spectra of **2**, **4**–**5**, Mössbauer spectra of **1b**, experimental and calculated values of ESI-MS signals for **2**–**5**, experimental IR carboxylate stretching vibrations (symmetric and asymmetric) for complexes **1**–**5**, experimental and expected effective magnetic moment values for **2**, **4**–**5**, UV/Vis spectra of **2**, **4**–**5** and corresponding λ_{max} and ε values, extended range CV of **1**, **2**, **4**, **5**, experimental and predicted ESI-MS values and IR spectra of **1b**, obtained by reaction of **1a** with $^{16}O_2$ and $^{18}O_2$.

Acknowledgements

This work was funded by the Deutsche Forschungsgemeinschaft (DFG, German Research Foundation) under Germany's Excellence Strategy (EXC 2008–390540038 – UniSysCat) and the Heisenberg-Professorship to K.R. Open access funding enabled and organized by Projekt DEAL.

Keywords: Heterobimetallic complex; Homobimetallic complex; Oxygen activation; Mössbauer spectroscopy; Reactive intermediates

References

[1] B. Battistella, K. Ray, *Coord. Chem. Rev.* **2020**, *408*, 213176.
[2] F. Heims, V. Mereacre, A. Ciancetta, S. Mebs, A. K. Powell, C. Greco, K. Ray, *Eur. J. Inorg. Chem.* **2012**, *2012*, 4565–4569.
[3] I. Garcia-Bosch, X. Ribas, M. Costas, *Eur. J. Inorg. Chem.* **2012**, *2012*, 179–187.
[4] M. E. Ahmed, A. Dey, *Curr. Opin. Electrochem.* **2019**, *15*, 155–164.
[5] C. Pathak, S. K. Gupta, M. K. Gangwar, A. P. Prakasham, P. Ghosh, *ACS Omega* **2017**, *2*, 4737–4750.
[6] P. V. Bernhardt, S. Bosch, P. Comba, L. R. Gahan, G. R. Hanson, V. Mereacre, C. J. Noble, A. K. Powell, G. Schenk, H. Wadepohl, *Inorg. Chem.* **2015**, *54*, 7249–7263.
[7] E. Gouré, M. Carboni, P. Dubourdeaux, M. Clémancey, R. Balasubramanian, C. Lebrun, P.-A. Bayle, P. Maldivi, G. Blondin, J.-M. Latour, *Inorg. Chem.* **2014**, *53*, 10060–10069.
[8] M. Carboni, M. Clémancey, F. Molton, J. Pécaut, C. Lebrun, L. Dubois, G. Blondin, J.-M. Latour, *Inorg. Chem.* **2012**, *51*, 10447–10460.
[9] J. B. Vincent, M. W. Crowder, B. A. Averill, *Trends Biochem. Sci.* **1992**, *17*, 105–110.
[10] M. B. Twitchett, A. G. Sykes, *Eur. J. Inorg. Chem.* **1999**, 2105–2115.
[11] E. Lambert, B. Chabut, S. Chardon-Noblat, A. Deronzier, G. Chottard, A. Bousseksou, J.-P. Tuchagues, J. Laugier, M. Bardet, J.-M. Latour, *J. Am. Chem. Soc.* **1997**, *119*, 9424–9437.
[12] R. M. Haas, Z. Hern, S. Sproules, C. R. Hess, *Inorg. Chem.* **2017**, *56*, 14738–14742.
[13] P. Karsten, A. Neves, A. J. Bortoluzzi, M. Lanznaster, V. Drago, *Inorg. Chem.* **2002**, *41*, 4624–4626.
[14] R. M. Buchanan, M. S. Mashuta, J. F. Richardson, R. J. Webb, K. J. Oberhausen, M. A. Nanny, D. N. Hendrickson, *Inorg. Chem.* **1990**, *29*, 1299–1301.
[15] T. R. Holman, Z. Wang, M. P. Hendrich, L. Que Jr., *Inorg. Chem.* **1995**, *34*, 134–139.
[16] S. K. Dutta, R. Werner, U. Flörke, S. Mohanta, K. K. Nanda, W. Haase, K. Nag, *Inorg. Chem.* **1996**, *35*, 2292–2300.
[17] M. Ghiladi, C. J. McKenzie, A. Meier, A. K. Powell, S. Wocadlo, *J. Chem. Soc. Dalton Trans.* **1997**, 4011–4018.
[18] S. Albedyhl, M. T. Averbuch-Pouchot, C. Belle, B. Krebs, J. L. Pierre, E. Saint-Aman, S. Torelli, *Eur. J. Inorg. Chem.* **2001**, 1457–1464.
[19] T. R. Holman, K. A. Andersen, O. P. Anderson, M. P. Hendrich, C. Juarez-Garcia, E. Münck, L. Que Jr., *Angew. Chem.* **1990**, *102*, 933–935.
[20] B. T. R. Holman, K. A. Andersen, O. P. Anderson, M. P. Hendrich, *Angew. Chem. Int. Ed. Engl.* **1990**, *29*, 921–923.
[21] M. Bedin, H. Agarwala, J. Marx, V. Schünemann, S. Ott, A. Thapper, *Inorg. Chim. Acta* **2019**, *490*, 254–260.
[22] A. L. Gavrilova, B. Bosnich, *Chem. Rev.* **2004**, *104*, 349–384.
[23] M. Carboni, M. Clémancey, F. Molton, J. Pécaut, C. Lebrun, L. Dubois, G. Blondin, J.-M. Latour, *Inorg. Chem.* **2012**, *51*, 10447–10460.
[24] F. R. Xavier, A. Neves, A. Casellato, R. A. Peralta, A. J. Bortoluzzi, B. Szpoganicz, P. C. Severino, H. Terenzi, Z. Tomkowicz, S. Ostrovsky, et al., *Inorg. Chem.* **2009**, *48*, 7905–7921.
[25] T. R. Holman, C. Juarez-Garcia, M. P. Hendrich, L. Que, E. Munck, *J. Am. Chem. Soc.* **1990**, *112*, 7611–7618.
[26] L. Yin, P. Cheng, S.-P. Yan, X.-Q. Fu, J. Li, D.-Z. Liao, Z.-H. Jiang, *J. Chem. Soc. Dalton Trans.* **2001**, 1398–1400.
[27] D. F. Evans, *J. Chem. Soc.* **1959**, 2003–2005.
[28] E. M. Schubert, *J. Chem. Educ.* **1992**, *69*, 62.
[29] C. Belle, I. Gautier-Luneau, G. Gellon, J.-L. Pierre, I. Morgenstern-Badarau, E. Saint-Aman, *J. Chem. Soc. Dalt. Trans.* **1997**, 3543–3546.
[30] D. L. Reger, C. A. Little, M. D. Smith, A. L. Rheingold, K.-C. Lam, T. L. Concolino, G. J. Long, R. P. Hermann, F. Grandjean, *Eur. J. Inorg. Chem.* **2002**, *2002*, 1190–1197.
[31] J. F. D. R. M. Golding, K. F. Mok, *Inorg. Chem.* **1966**, *5*, 774–778.
[32] This trend is, however, not obvious in the absorption spectra of the complexes (Figure S3, Table S4, Supporting Information). The lowest energy transition occurs at 559 nm for **2**, 524 nm for **4**, and 597 nm for **5**. For **1**, as previously reported,[2] it occurs at 500 nm. Thus the energy of the lowest energy transition does not

systematically reflect the electrophilicity of the M^{II} ion in this series of Fe^{III} M^{II} (M = Mn, Co, Ni and Cu) complexes.
[33] J. Annaraj, Y. Suh, M. S. Seo, S. O. Kim, W. Nam, *Chem. Commun.* **2005**, 4529–4531.
[34] D. L. Wertz, J. S. Valentine, *Struct. Bonding (Berlin)* **2000**, *97*, 37–60.
[35] S. Graham-Lorence, B. Amarneh, R. E. White, J. A. Peterson, E. R. Simpson, *Protein Sci.* **1995**, *4*, 1065–1080.
[36] B. P. Murch, F. C. Bradley, P. D. Boyle, V. Papaefthymiou, L. Que, *J. Am. Chem. Soc.* **1987**, *109*, 7993–8003.
[37] S. Ménage, J.-B. Galey, J. Dumats, G. Hussler, M. Seité, I. G. Luneau, G. Chottard, M. Fontecave, *J. Am. Chem. Soc.* **1998**, *120*, 13370–13382.
[38] G. M. Mockler, J. De Jersey, B. Zerner, C. J. O'Connor, E. Sinn, *J. Am. Chem. Soc.* **1983**, *105*, 1891–1893.
[39] M. N. Mortensen, B. Jensen, A. Hazell, A. D. Bond, C. J. McKenzie, *Dalton Trans.* **2004**, 3396–3402.
[40] P. Comba, R. Cusack, D. P. Fairlie, L. R. Gahan, G. R. Hanson, U. Kazmaier, A. Ramlow, *Inorg. Chem.* **1998**, *37*, 6721–6727.
[41] J. K. Eberhardt, T. Glaser, R.-D. Hoffmann, R. Fröhlich, E.-U. Würthwein, *Eur. J. Inorg. Chem.* **2005**, *2005*, 1175–1181.
[42] K. D. Karlin, J. C. Hayes, Y. Gultneh, R. W. Cruse, J. W. McKown, J. P. Hutchinson, J. Zubieta, *J. Am. Chem. Soc.* **1984**, *106*, 2121–2128.
[43] K. E. Litz, M. M. Banaszak Holl, J. W. Kampf, G. B. Carpenter, *Inorg. Chem.* **1998**, *37*, 6461–6469.
[44] N. W. Aboelella, E. A. Lewis, A. M. Reynolds, W. W. Brennessel, C. J. Cramer, W. B. Tolman, *J. Am. Chem. Soc.* **2002**, *124*, 10660–10661.
[45] N. W. Aboelella, J. T. York, A. M. Reynolds, K. Fujita, C. R. Kinsinger, C. J. Cramer, C. G. Riordan, W. B. Tolman, *Chem. Commun.* **2004**, 1716–1717.
[46] J. T. York, A. Llobet, C. J. Cramer, W. B. Tolman, *J. Am. Chem. Soc.* **2007**, *129*, 7990–7999.
[47] J. T. York, V. G. Young, W. B. Tolman, *Inorg. Chem.* **2006**, *45*, 4191–4198.
[48] S. Kundu, F. F. Pfaff, E. Miceli, I. Zaharieva, C. Herwig, S. Yao, E. R. Farquhar, U. Kuhlmann, E. Bill, P. Hildebrandt, et al., *Angew. Chem.* **2013**, *125*, 5732–5736.
[49] S. Kundu, F. F. Pfaff, E. Miceli, I. Zaharieva, C. Herwig, S. Yao, E. R. Farquhar, U. Kuhlmann, E. Bill, P. Hildebrandt, et al., *Angew. Chem. Int. Ed.* **2013**, *52*, 5622–5626.
[50] E. Kim, E. E. Chufán, K. Kamaraj, K. D. Karlin, *Chem. Rev.* **2004**, *104*, 1077–1133.
[51] E. E. Chufán, S. C. Puiu, K. D. Karlin, *Acc. Chem. Res.* **2007**, *40*, 563–572.
[52] M. J. Gunter, L. N. Mander, K. S. Murray, *J. Chem. Soc., Chem. Commun.* **1981**, 799–801.
[53] Z. Halime, H. Kotani, Y. Li, S. Fukuzumi, K. D. Karlin, *Proc. Natl. Acad. Sci. USA* **2011**, *108*, 13990–13994.
[54] R. A. Brand, *Nucl. Instr. Methods B* **1987**, *28*, 398–416.
[55] G. M. Sheldrick, *Acta Crystallogr. Sect. A* **2015**, *71*, 3–8.
[56] G. M. Sheldrick, *Acta Crystallogr. Sect. C* **2015**, *71*, 3.

Received: May 19, 2020

